IOP Publishing Nanotechnology
Journal **XX** (XXXX) XXXXXX https://doi.org/XXXX/XXXX

Cytocompatibility of Carboxylated Multi-wall Carbon Nanotubes in Stem Cells from Human Exfoliated Deciduous Teeth

Eduarda R. Oliveira[1]; Leonara Fayer[1]; Rafaella S. S. Zanette[1]; Luiz O. Ladeira[2]; Luiz F. C. de Oliveira[3], Carlos M. C. Maranduba[4], Humberto M. Brandão[5]; Michele Munk[1*]

[1] Laboratory of Nanobiotechnology and Nanotoxicology, Department of Biology, Federal University of Juiz de Fora, Brazil.
[2] Nanomaterials Laboratory, Department of Physics, Federal University of Minas Gerais, Brazil.
[3] Nucleus of Spectroscopy and Molecular Structure, Department of Chemistry, Federal University of Juiz de Fora, Brazil
[4] Laboratory of Human Genetics and Cell Therapy, Department of Biology, Federal University of Juiz de Fora, Brazil.
[5] Laboratory of Nanotechnology, Brazilian Agricultural Research Corporation- Embrapa Dairy Cattle, Brazil.

*E-mail: michele.munk@icb.ufjf.br

Received xxxxxx
Accepted for publication xxxxxx
Published xxxxxx

Abstract

Carboxylated Multi-wall Carbon Nanotube (MWCNT-COOH) presents unique properties due to nanoscale dimensions and permits a broad range of applications in different fields, such as bone tissue engineering and regenerative medicine. However, the cytocompatibility of MWCNT-COOH with human stem cells is poorly understood. Thus, studies elucidating how MWCNT-COOH affects human stem cell viability are essential to a safer application of nanotechnologies. Using stem cells from the human exfoliated deciduous teeth model, we have evaluated the effects of MWCNT-COOH on cell viability, oxidative cell stress, and DNA integrity. Results demonstrated that despite the decreased metabolism of mitochondria, MWCNT-COOH had no toxicity against stem cells. Cells maintained viability after MWCNT-COOH exposure. MWCNT-COOH did not alter the superoxide dismutase activity and did not cause genotoxic effects. The present findings are relevant to the potential application of MWCNT-COOH in the tissue engineering and regenerative medicine fields.

Keywords: Carbon Materials, In Vitro Study, Nanotechnology, Tissue Engineering.

1. Introduction

The carbon nanotube is considered one of the most important nanomaterials (NM) known to man. Notably, the Multi-wall Carbon Nanotube (MWCNT) has attracted immense attention due to its chemical stability, thermal and electrical conductivity, mechanical strength, high surface area, flexibility, capillarity, lightweight, and bioactivity [1–3]. Modification of MWCNT with carboxyl group is one of the widely used approaches to increase their bioactivity. These appealing properties make them potentially adequate for the biomedical field and other industries [4–6]. They have also been utilized for imaging, bioengineering, tissue regeneration, and regenerative medicine [4–7]. MWCNTs have been used to construct biosensors and vectors for drug and gene delivery [8-10] and are promising vectors for nano-vaccinology [11]. Nanoscaffolds have been developed utilizing MWCNT due to their capacity to enhance the polymer mechanical strength and electrical conductivity in neuronal and bone tissue repair studies [12,13].

Even though MWCNTs hold great promise for various applications for biomedicine, nanoscale confers a higher reactivity to NMs because they present a high surface area. Thus, when in contact with biological systems, NMs may cause toxicity [14]. Then, nanotoxicity is a critical factor that limits nanotechnology. There is a consequent increase in the release and exposure of carbon nanotubes since they are the most widely used NM. Carbon nanotubes can enter cells via membrane adsorption, phagocytosis, pinocytosis, and endocytosis [15]. Once into the cells, they can cause various cellular responses that lead to toxicity. As examples, these NMs might induce reactive oxygen species (ROS), inducing apoptosis and DNA damage [2]. Consequently, animal and human exposition due to technologies using carbon nanotubes are more significant [16,17].

Recently investigators have examined the effects of different MWCNTs on mammalian stem cells. Song *et al* [18] demonstrated that MWCNT was toxicity for bone mesenchymal stem cells in rats. Mia *et al* [19] found that the acid-functionalized single-walled carbon nanotubes stimulated ROS production on bone marrow-derived hematopoietic stem cells. Mooney *et al* [20] shown that MWCNT decreased the cell viability of human mesenchymal stem cells. Nevertheless, Das *et al* [21] registered that MWCNT-COOH was cytocompatible for canine mesenchymal stem cells. According to Kroustalli and Deligianni [22], the MWCNT induced human mesenchymal stem cell proliferation. Therefore, a gap still needs to be filled with studies that examine the cytocompatibility of MWCNTs in human stem cells. In addition, we need to expand our current knowledge in this field.

Stem cells from human exfoliated deciduous teeth (SHED) are multipotent cells that can self-renew and differentiate into several phenotypes. These cells have been regarded as critical for cell therapy in the field of regenerative dentistry and medicine. In this context, controlling the fate of stem cells is one of the most studied tissue engineering issues. For this purpose, the MWCNT-COOH can enhance stem cells interactions for tissue regeneration as a culture substrate. Previous studies have shown that carbon nanotubes can increase the substrate surface roughness interacting with extracellular matrix proteins, such as fibronectin and vitronectin [23], increasing tissue regeneration capacity.

Moreover, stem cells are widely used for toxicological screening because of their sensitivity to potential toxicants. The higher sensitivity of stem cells than somatic cells is related to their capacity to differentiate in vitro into multi-cell types under defined conditions. They are unspecialized and more sensitive to environmental stimuli so that traditional cytotoxicity assays can generate highly informative data [24]. Therefore, stem cells and their responses to the *in vitro* environment in which they are growing can serve as windows to understand the potential effects of NM with potential biotechnological applications.

Thus, the investigation of the effect of MWCNT-COOH on SHED cells could provide new evidence for safer and better use of MWCNT-COOH as platforms for tissue engineering and regenerative medicine, in addition to expanding our current knowledge in this field.

This work investigated whether the MWCNT-COOH affects viability, oxidative metabolism, and DNA integrity using SHED cells as a stem cell model. For this purpose, we synthesized and characterized MWCNT-COOH via Fourier Transformed Infrared (FTIR), Raman, atomic force microscopy (AFM), transmission electron microscopy (TEM), dynamic light scattering (DLS), and Zeta Potential (ZP) techniques. The cell metabolism and cytotoxicity were tested by light microscopy, thiazolyl blue tetrazolium blue (MTT), flow cytometry, and superoxide dismutase (SOD) activity assays. The genotoxicity was analyzed via a micronucleus test. We demonstrate for the first time that MWCNT-COOH is cytocompatible with SHED cells. The results provide new insights into the safer use of MWCNT-COOH in the tissue engineering and regenerative medicine fields.

2. Materials and Methods

2.1 Materials

Dulbecco's Modified Eagle Medium-F12 (DMEM-F12), trypsin-EDTA, propidium iodide (IP), cytochalasin β (cyto β), thiazolyl blue tetrazolium blue (MTT), superoxide dismutase (SOD) assay kit, cyclophosphamide, methyl methanesulphonate, and Giemsa were purchased from Sigma-Aldrich, USA. The fetal bovine serum (FBS) and penicillin-streptomycin antibiotics were acquired from LGC Biotechnology, Brazil. Phosphate-buffered saline (PBS) was purchased from Gibco Laboratories, UK.

2.2 Synthesis of MWCNT-COOH

The MWCNT synthesis was made via the floating catalytic chemical vapor deposition technique, using Al_2O_3-Co-Fe to catalyze the process. After the synthesis, the MWCNTs were heated at 400 °C for 50 min under atmospheric conditions to eliminate amorphous carbon structures. Then, MWCNTs were treated with HCl for 24 h to reduce the Fe_2O_3 and Co_2O_3 to less the 1% of the carbon content. After, the MWCNT surface was functionalized with carboxyl (-COOH) groups through nitric/sulfuric (3:1) acid oxidation for 2-4 h. This process also eliminates more Fe and Co content, and only traces of these metals remain. Several centrifugations in water suspensions were made to remove the acids of MWCNT-COOHs and reach a neutral pH (6.5-7.0). Then, the MWCNT-COOHs were dried for 12 h. The obtained MWCNT-COOHs showed 8-10% of carboxyl group concerning the carbon content, purity >93%, presented <2% of other structures, and <5% of contaminants from the synthesis.

2.3 Characterization of MWCNT-COOH

2.3.1 Chemical analysis of MWCNT-COOH.

To chemically characterize the MWCNT-COOH, we performed two complementary techniques. First, we executed the FTIR spectroscopy, and for that, we obtained the absorption spectra in the infrared region on a Bomem FT IR MB-102 spectrometer (Bomem, Canada). The absorptions occurred in a wavelength range from 3000 cm^{-1} to 500 cm^{-1}, utilizing KBr tablets previously desiccated at 500°C. Second, we captured the Raman spectra on a Bruker Senterra spectrometer (Bruker, USA). A dry sample of the MWCNT-COOH was put on a microscope slide and submitted to a 632.8 nm laser at 10 mV potency for 15 sec. Acquisitions were made 20 times with a spectral resolution of 3-5 cm^{-1}, in a 50x objective. The experiments were conducted in triplicates.

2.3.2 Morphological evaluation of MWCNT-COOH.

Images of TEM and AFM were obtained for morphological evaluation of the MWCNT-COOHs. TEM images were taken

on a Tecnai G2-20 microscope (FEI Company, USA) at a 220 kV voltage and 3 mm spot size. Copper grids Holey Carbon was used for the deposition of the MWCNT-COOHs samples. For that, one drop of a mother solution was diluted in 5 mL of deionized water. The new suspension was submitted to a 5-min ultrasound bath, and a drop was put on the copper grid. After, the grid was left for drying in an incubator at 70ºC for 12 h. We acquired AFM images of a dry sample of MWCNT-COOHs on a Nanosurf EasyScan 2 microscope (Nanosurf Instruments, Swiss) via intermittent mode. The resultant images were utilized to define the diameter of the nanomaterial using ImageJ (Wayne Rasband) software.

2.3.3 Dynamic Light Scattering and Zeta Potential evaluation.

To get insights into how MWCNT-COOHs behave in an aqueous medium and its liquid charge, DLS and Zeta Potential analysis of suspensions containing MWCNT-COOHs at 0, 0.1, 1, 10, 50, 100 μg mL^{-1} were determined on a Malvern 3000 Zetasizer NanoZS (Malvern Instruments, UK). The chosen NM concentrations are close to a realistic exposure (up to 100 μg mL^{-1}) and have been used in previous works [25-29]. Furthermore, all concentrations of MWCNT-COOHs were freshly prepared in three types of aqueous medium: deionized water (pH 7.1), DMEM-F12 (pH 6.9-7.1), and DMEM-F12 supplemented with FBS (10% v/v) (pH 6.9-7.1). The refractive index of MWCNT-COOH used in DLS analysis was 1.891 [30].

2.4 Cytocompatibility analysis of MWCNT-COOH

2.4.1 Cell culture and co-incubation with MWCNT-COOH.

SHEDs were obtained from Human Genetics and Cell Therapy Biobank (GENETEC) at the Federal University of Juiz de Fora. All proceedings were performed as per the ethical standards of the local ethics committee (CEP/UFJF No. 003/2011 and CAAE No 27681214.7.0000.5147). The SHEDs were previously characterized as published in Ferreira *et al* [31]. The SHEDs were cultured in a DMEM-F12 growth medium supplemented with antibiotics (100 U mL^{-1} penicillin and 100 mg mL^{-1} streptomycin) and FBS (10% v/v). Then, cells were incubated in a Thermo Scientific Forma Series 3 Water Jacketed CO_2 incubator (Thermo Scientific, USA), a humidified atmosphere containing 5% CO_2 at 37ºC. The culture medium was changed every 3 days. Subculturing occurred when around 80% confluence was achieved, detaching cells by trypsinization. For all cytotoxic and genotoxic assays, cells were exposed to 0 (control), 0.1, 1, 10, 50, 100 μg mL^{-1} of MWCNT-COOH freshly dispersed in supplemented DMEM-F12 and incubated for 24, 42, and 72 h. Before cell exposure, the MWCNT-COOH was dispersed with a UP200S sonicator (Hielscher, Germany) set in amplitude 75 and cycle 0.5, for approximately 1 min. All the experiments were conducted in triplicates and repeated three times unless otherwise stated.

2.4.2 Cell morphology and spreading area analysis.

We analyzed cell morphology and the area of cell spreading in monolayers through an inverted light microscope. SHEDs ($3x10^3$ cells/well) were seeded in a 6-well plate and exposed to MWCNT-COOH for 24, 48 and 72 h according to ISO 10993-5 (ISO2009) [32]. Analysis of cell shape and images were taken on a Zeiss PrimoVert inverted microscope (Carl Zeiss, Germany). Cell perimeter was manually measured using ImageJ (Wayne Rasband). This app feature generated the cell area automatically. The sample size for each treatment was n= 100 and included a minimum of five different observation fields.

2.4.3 Mitochondrial activity analysis.

Cells ($3x10^3$ cells/well) were seeded in a 96-well plate and exposed to MWCNT-COOHs for periods of 24, 48, and 72 h. After the exposure, the growth medium was removed, and cells were washed with 1X PBS three times to remove the excess of NM that could interfere with the absorbance reading. After, 200 μl of DMEM-F12 containing MTT (stock solution 5 mg ml^{-1}) (10% v/v) was added to each well. Cells were incubated for 4 h at 37 °C in 5% CO_2 humidified atmosphere. Afterward, the MTT solution was discarded, and 200 μl of acid isopropyl alcohol was added. The plate was incubated for 1 h at 37 °C. Then, acid isopropyl alcohol was resuspended to dissolve the formazan crystals. Absorbance was measured at 570 nm in a Varioskan Flash Multimode Reader spectrophotometer (Thermo Scientific, USA).

2.4.4 Oxidative stress analysis.

The SODs are antioxidant enzymes that protect cells against oxidative stress. According to the manufacturer's instructions, the SOD activity was determined via a spectrophotometric method using a SOD assay kit (Sigma-Aldrich, USA). Briefly, cells ($5x10^3$ cells/well) were seeded in a 96-well plate and exposed to MWCNT-COOHs for 24, 48 and 72 h. After the exposure time, the growth medium was removed, cells were washed three times using 1x PBS for MWCNT-COOHs removal and trypsinized. Then, cells were collected by centrifugation at 2000 g for 10 min, 4 ºC, washed twice with 1 ml of 1x PBS, and centrifuged under the same conditions. Supernatants were discarded, and cells were lysed by the freezing and thawing method. Pellets were resuspended in 100 μl 1x PBS. Afterward, 20 μl of the suspension was used to proceed to assay according to kit instructions. The colorimetric change was detected using Varioskan Flash Multimode Reader spectrophotometer (Thermo Scientific, USA) at 450 nm of absorbance.

2.4.5 Cell viability analysis.

The SHEDs ($3x10^4$ cells/well) were seeded in a 6-well plate and exposed to MWCNT-COOHs for 24, 48 and 72 h. After treatment, the growth medium was removed, and the cells were washed with 1X PBS three times and trypsinized. Cells were collected by centrifugation at 1500 rpm for 5 min. Then,

the cells were resuspended in 1x PBS and stained with PI (50 µg mL^{-1}). The cell suspensions were read in a CytoFLEX S cytometer (Beckman Coulter, USA). The experiments were performed in triplicates and repeated three times.

2.4.6 Genotoxicity analysis.

The genotoxic potential of MWCNT-COOHs was determined by micronuclei assay, according to the Organisation for Economic Co-operation and Development (OECD) adapted protocol (TG 487) [33]. Two positive controls were used as clastogenic agents: Cyclophosphamide (5 µg mL^{-1}) and Methyl Methane Sulphonate (3 µg mL^{-1}). Besides the negative control (0 µg mL^{-1} MWCNT-COOH) and MWCNT-COOH treatments (0.1, 1, 5 and 10 mL^{-1}). All groups received Cyto β at 3µg mL^{-1} during the 24 h exposure, ensuring binucleated cell formation. Then, cells were washed three times with 1x PBS, trypsinized, and centrifuged at 120 g for 5 min. For fixation, 300 µl of KCl (0.075 M) was added, followed by another centrifugation at 1000 rpm for 5 min). Then, the pellet was resuspended in 100 µl of Carnoy fixer.

Slides were prepared using the smear technique. After air drying, slides were put under clearing solution (acetic acid 45%) for 10 sec and stained with Giemsa (5%) for 10 min. During slide analysis, a total of 500 cells per group were counted and distinguished between mono, bi, and multinucleated cells to calculate CBPI (Cytokinesis-block proliferation index). For micronuclei frequency analysis, 2000 binucleated cells per group were counted. The experiments were performed in triplicates and repeated three times.

2.5 Statistical analysis

Data were analyzed in GraphPad Prism 5.0 (GraphPad Software, USA). One-way ANOVA followed by Tukey's test for means comparison was applied to cell morphology, cell viability, mitochondrial activity, and oxidative stress data. A Chi-square test was performed to analyze Micronuclei results. Differences between groups were considered statistically significant when $p < 0.05$. Numerical data are presented as the mean ± standard error of the mean.

3. Results and Discussion

3.1 Chemical characterization of MWCNT-COOH

Before the biological assays, it is necessary to perform the NM characterization due to some insights into the NM interaction mechanisms in biological systems. Therefore, we carried out the physical-chemical characterization of the MWCNT-COOH by FTIR, Raman, AFM, TEM and DLS analysis.

In general, carbon nanotubes have a chemical composition consisting of graphite and impurities intrinsic to the synthesis process. Consequently, it may present marked insolubility, hindering its dispersion in the aqueous medium. Thus, carbon nanotubes tend to form aggregates and may trigger toxicity when interacting with organisms [34]. Previous works demonstrate that pristine MWCNTs are cytotoxic to rat bone marrow stem cells [18, 35]. Hence, it is usual to chemically treat carbon nanotubes to promote a more significant contact with the atoms and molecules of the fluid and improve solubility [34]. Thus, carboxylation is used to modify the MWCNT surface and enhance its dispersion [36]. In the present study, we utilized FTIR and Raman techniques to characterize the MWCNT-COOHs chemically (Figure 1). FTIR spectra are ranging from 500 to 3000 wavenumber/cm^{-1} (Figure 1A). We observed the peaks 1643 cm^{-1}, 1734 cm^{-1} and 1391 cm^{-1}. These values are according to previous studies [37–40]. The peak seen at 1643 cm^{-1} is characteristic of vibrations from bonds between carbon atoms that form the hexagonal net found in graphite sheets that build carbon nanotubes [37]. The peak at 1734 cm^{-1} represents the vibration aspects of a C=O bond found in carboxyl groups [39, 41]. The 1391 cm^{-1} peak stands for the typical vibration of hydroxyl groups (-OH), also referring to the functionalization [40]. It is possible to observe two values referring to the same chemical group (-COOH) since it may be linked to the carbon nanotube walls in different directions, reflecting different FTIR readings. The FTIR data confirm, therefore, the presence of carboxyl groups from the functionalization.

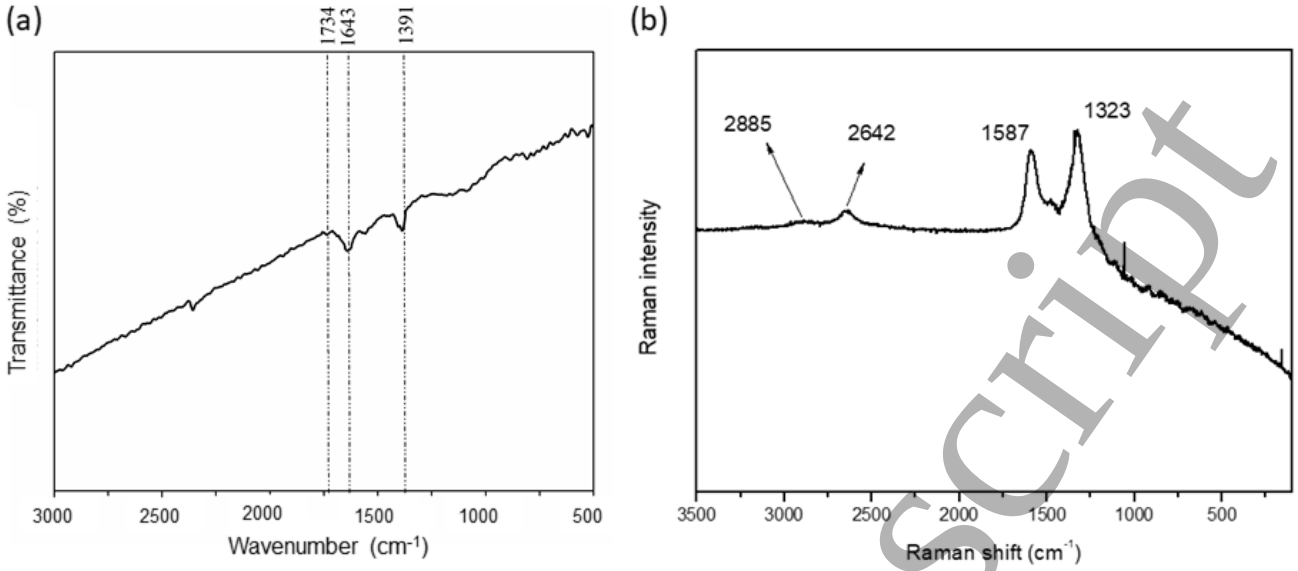

Figure 1. (a) Carboxylated Multi-Walled Carbon Nanotubes (MWCNT-COOH) infrared spectra ranging from 500 to 3000 wavenumber/cm^{-1}. The peaks 1643 cm^{-1} of carbon atoms, 1734 cm^{-1} of carbon-oxygen (C=O) bonds, and 1391 cm^{-1} of hydroxyl groups (-OH) are observed. The Fourier Transformed Infrared (FTIR) data confirm the carbon composition of the MWCNT and the functionalization with carboxyl groups (-COOH). (b) Raman Spectroscopy of MWCNT-COOH. Raman shifts range from 0 to 3500 cm^{-1}. The peak at 1587 cm^{-1} is the G band of carbon atoms. The peaks at 1323 and 2642 cm^{-1} are the D and the D` bands of structural bond's distortions from amorphous carbons.

Raman results provided information on the chemical composition of the MWCNT-COOHs and are presented in Figure 1B. Raman shifts range from 0 to 3500 cm^{-1}. The peak at 1587 cm^{-1} is the G band and relative to atomic vibrations of bonds between carbon atoms found in structures formed by graphite, like carbon nanotubes. The peaks seen at 1323 and 2642 cm^{-1} are the D and the D` bands, respectively, of structural bond distortions from amorphous carbons and alterations in the hexagonal structure formed by carbons. Our results agree with those found in the literature showing that D-bands is at 1320-1370 cm^{-1} are present in carbon nanotube [39,40]. The chemical characterization of carbon nanotubes by Raman Spectroscopy is broadly used. However, most of these spectrum characteristics that differentiate the graphite structure from the MWCNT structure are not evident. The G band is related to the vibrations of the carbon atoms of the graphitic structure (so the band is named G). It is a unique and intense peak. Single Wall Carbon Nanotubes have a spectrum containing a G band with two peaks (G+ and G-), distinguishing these nanotubes of graphite. In turn, the single G band appearance in MWCNTs occurs due to the larger and various diameter sizes formed by the graphite concentric layers that characterize this type of nanotube [42,43]. We also observe a change in Raman intensity in the region of low-frequency wavelengths (100-200 cm^{-1}), which relates to a radial breathing mode of carbon atoms. Radial breathing mode is strongly associated with the wider diameter from the multiple layers of MWCNTs [43-46]. In the present study, Raman spectroscopy data along with FTIR confirmed the MWCNT chemical composition.

3.2 Morphological characterization of MWCNT-COOH

The morphology of the MWCNT-COOH was analyzed by TEM and AFM techniques (Figure 2). In Figure 2B, we show the MWCNT-COOHs through the TEM. We observed the hollowed nanofiber structures of the MWCNT-COOHs with a 17.7 nm average diameter. Moreover, the MWCNT-COOHs displayed some surface irregularities indicated by dashed ellipses. The AFM image contains MWCNTs with their typical elongated shape (Figure 2C). The diameter of these MWCNT-COOHs ranged from 10 to 20 nm.

TEM and AFM results together show that the MWCNT-COOHs dimensions are in concordance with what was reported in the literature [47,48]. The dimensions presented by these MWCNT-COOHs can contribute to a good viscosity of scaffolds since this characteristic is associated with size and height/length that influence the Brownian motion. Omrani [48] revealed that an MWCNT-COOH with a lower length/diameter ratio provides greater viscosity to nanofluids. Suitable viscosity is a relevant characteristic for tissue bioengineering applications since it allows the transport of molecules and gases through fluid materials [49–51]. Therefore, the MWCNT-COOH is a pertinent NM applicable to the improvement of scaffolds for cell growth.

Additionally, we observed some regions of superficial irregularities in TEM images, which suggest changes in the surfaces of MWCNT-COOHs. Surface changes can be correlated with the intensity of band D seen in Raman spectroscopy. Wepasnick *et al* [44] reported the interrelationship between strong oxidants for the addition of COOHs groups, quantities of these groups linked to the

MWCNT wall, irregularities in the NM surface, and the existence of amorphous carbons with the intensity of the D band. Van Trinh *et al* [34] have already related the increase in the time of the functionalization process by chemical treatments (acidifiers and oxidizers) that form covalent bonds (like COOHs bonding on the surface of MWCNTs) with the increase of superficial alterations and the D band in Raman spectroscopy. According to Wepasnick *et al* [44], these irregularities on the NM surface may indicate sites of carboxyl groups linkage. In concordance with these previous findings, we can also correlate the TEM data with the strong intensity of the D band observed in Raman, suggesting the functionalization of the MWCNT.

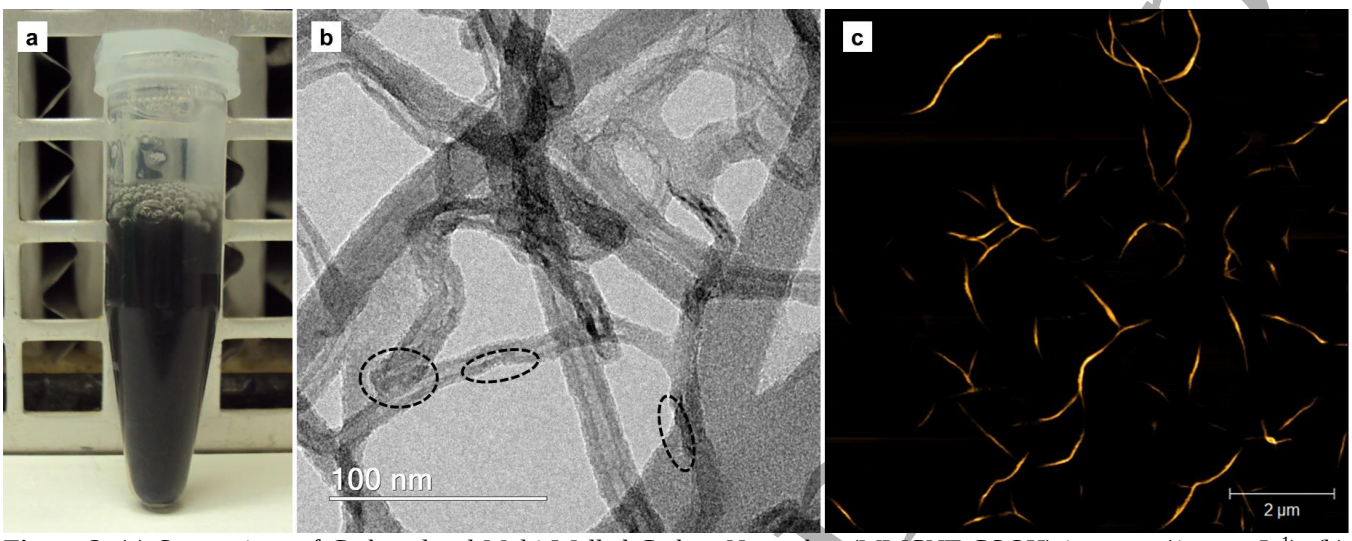

Figure 2. (a) Suspensions of Carboxylated Multi-Walled Carbon Nanotubes (MWCNT-COOH) in water (1 mg mL^{-1}), (b) Transmission Electron Microscopy, and (c) Atomic Force Microscopy images of MWCNT-COOHs. Dashed ellipses signal surface irregularities. Scale bar = 100 nm e 2 µm.

3.3 DLS and ZP evaluation

We performed the DLS and ZP assays to be aware of the dispersion behavior and the superficial net charge of the MWCNT-COOH since these are parameters that can interfere in the interaction of the NM with the cells. In table 1, we display the hydrodynamic size, polydispersity index (PDI) and ZP results. Different MWCNT-COOH concentrations (0.1, 1, 10, 50, 100 µg mL^{-1}) were dispersed in three types of aqueous medium: deionized water, DMEM/F12 and DMEM/F12 + FBS (10% v/v). This procedure helps to understand how the molecules that compose the growth medium can influence the NMs dispersion. We observed that the hydrodynamic size values were high for all five concentrations of MWCNT-COOH when dispersion was in deionized water (from 1575.3 to 5589.0 nm). The dispersion results in DMEM/F12 were between 1198.3 and 3752.7 nm, and therefore, lower than dispersion in deionized water. However, hydrodynamic size decreased when MWCNT-COOHs were dispersed in DMEM/F12 supplemented with FBS, exhibiting 62.7 to 211.4 nm. In general, the hydrodynamic diameters showed aggregation as a function of MWCNT-COOH concentration in deionized water and DMEM/F12. In these cases, Van der Waals overcome the repulsive electrostatic forces, leading to different sizes of MWCNT-COOH aggregates [52]. DMEM/F12 + FBS (10% v/v) was more effective in dispersing the MWCNT-COOHs, providing hydrodynamic sizes smaller than 100 nm. This higher dispersibility is due to the FBS proteins, mainly albumin and other culture medium constituents, that influence the behavior related to aggregation and dispersion of NMs [53,54]. Albumin tends to form a protein corona, interacting electrostatically with carbon nanotubes and free carboxylic groups. Carboxylation allows bonds with various functional molecules such as drugs, oligonucleotides, and proteins. Therefore, the MWCNT-COOHs can be less hydrophobic and more stable due to the formation of the protein corona [36]. In the present study, the growth media cell culture was supplemented with FBS. Thus, the MWCNT-COOHs should form smaller aggregates. However, when the analysis of MWCNT-COOHs concentrations was performed within the same group of the aqueous medium, we observed that the higher concentrations (50 and 100 µg mL^{-1}) presented the largest hydrodynamic sizes. In this case, the aggregates can also be due to the greater availability of MWCNT-COOHs in the suspension. Previous findings state that the higher NM concentration induces aggregate formation [55–57].

The PDIs of MWCNT-COOH at different concentrations (0.1, 1, 10, 50, 100 µg mL^{-1}) and dispersed in three different media (deionized water, DMEM/F12 and DMEM/F12 FBS) varied between 0.2 and 1.0 (Table 1). PDI is an estimative of the average uniformity of a particle solution. Our results show that most of the treatments had an intermediary polydispersity level ($0.3 \geq PDI \leq 0.6$). The treatments 0.1 and 10 µg mL^{-1} in deionized water, 1 and 50 µg ml^{-1} in DMEM/F12, and 0.1 µg

mL^{-1} in DMEM/F12 FBS had a heterogenic distribution of the hydrodynamic size (PDI≥0.7). The treatments 100 μg mL^{-1} in DMEM/F12 and 0.1 μg mL^{-1} in DMEM/F12 FBS presented a monodispersed population (≥0.3), and therefore, a homogenous size distribution [58].

In table 1, we show the ZP results. All MWCNT-COOH treatments displayed a negative net charge at pH 7.1. Only one exception for the concentration of 0.1 μg mL^{-1} in deionized water had a ZP of 0.2 ± 0.9 mV. The concentration of 100 μg mL^{-1} MWCNT-COOH suspended in DMEM/F12 (-27.87 mV) is the most stable suspension among the evaluated groups. Besides, we observed that the ZP value declined as the MWCNT-COOH concentration increased. ZP is an index of the magnitude of electrostatic interaction between colloidal particles. Furthermore, studies suggest a change in surface charge and ZP due to functionalization, indicating that it may cause particles to be more or less interactive [59]. Therefore, the functionalization confirmed by FTIR can explain the obtained negative values of the ZP. In addition, since the surface hydrophilicity of NM is directly related to their cytocompatibility, we and used the ZP measurement to evaluate the electrostatic interaction between MWCNT-COOHs and water. High ZP values are important for increasing NM interactions with the water molecules, reducing their hydrophobicity, and formation of aggregates. These properties are related to better cytocompatibility of NMs [59-61]. In the present study, MWCNT-COOH showed a high ZP value (-27.87 mV) and a particle size between 62.7 and 211.4 nm in DMEM/F12 medium, with fewer aggregates. We also observed good dispersibility of MWCNT-COOH in water (Figure 2A), which indicates hydrophilicity. The ZP results indicate that the MWCNT-COOH is electrically charged in the aqueous medium, preventing aggregation by electrostatic repulsion. Therefore, these DLS and ZP results can impact on good cytocompatibility of the MWCNT-COOH.

Our results agree with other studies that evaluated carboxylated carbon nanotubes, non-functionalized, or presented other functionalization [9,60,61]. However, Bai *et al* [36] reported ZP values of functionalized carbon nanotubes greater than -35 mV, while the non-functionalized ones presented -14 mV. Lee *et al* [52] had similar results. Therefore, the variation in the ZPs may be due to the conditions of NMs synthesis and its contaminants (such as catalysts), pH, functionalizing groups on the surface, growth medium, and other factors.

3.4 Cytocompatibility analysis of MWCNT-COOH

3.4.1 Cell morphology and spreading area analysis.

Optical microscopy observation was first used to evaluate the cell morphology and the cell spreading area in monolayer culture. Figures 3, 4 and 5 show the results of the cell morphology analysis after MWCNT exposure for 24, 48 and 72h. We verified that SHED cells grew in adherent monolayer and displayed their fibroblast-like typical morphology and elongated and fusiform shape, or sometimes a triangular, flattened starry form [62]. On the other hand, rat bone marrow stem cells exposed to pristine MWCNTs for the same periods presented an apoptotic morphology [18].

Figure 6 shows aggregates of MWCNT-COOH in SHEDs culture. Notably, the most visible and larger aggregates tend to contact and interact with SHED cells, as pointed out by arrows. The typical fusiform shape was maintained in all treatments. Nevertheless, we verified that the cell spreading area was reduced in some treatments compared to the control (Figure 7).

The reduction of the cellular spreading area occurred after 24h and 72 h of exposure to higher concentrations (50 and 100 μg mL^{-1}) of MWCNT-COOH ($p>0.05$). On the other hand, 48h exposure decreased cell spreading area in all treatments ($p>0.05$), except for 1 μg mL^{-1}. This reduction of the growing cell area in adherent monolayer may be related to the interaction of MWCNT-COOH aggregates with the cell membrane, as we observed in light microscopy (Figure 6). Literature shows that oxidized MWCNTs tend to be adsorbed in the membrane of vesicles composed of lipid bilayers (cell membrane-like) and interact with the polar portion of phospholipids [63]. On the other hand, previous studies have shown that cell morphology changes may be related to the differentiation process [64–66]. Thus, we can suggest a correlation between the cell morphology alteration observed in this study and possible cell differentiation. Also, a previous study revealed that MWCNT-COOH induced the neural differentiation of human bone marrow mesenchymal stem cells [67]. However, that correlation should be better evaluated in future studies.

3.4.2 Mitochondrial activity analysis.

Since NM can interfere in the mitochondrial metabolism of cells, we conducted an MTT assay to evaluate the mitochondrial activity of SHEDs exposed to MWCNT-COOH. Figure 8 shows that MWCNT-COOH reduced formazan crystals formation ($p<0.05$). This reduction in a cell exposed to NM indicates less mitochondrial activity compared to the control group. Similarly, rat stem cells also presented reduced values after exposure to 10 μg mL^{-1} of non-functionalized MWCNT [18].

Data from the literature report induction of cytotoxicity by carbon nanotubes via a decrease in mitochondrial activity in different cell types [26-28]. Previous data revealed that MWCNT-COOH reduced the mitochondrial activity of human lung bronchial cells at concentrations of 20, 40 and 100 μg mL^{-1} [26]. However, the treatments 0.1 and 1 μg mL^{-1} did not affect the mitochondrial activity of human spermatozoa [27] and concentrations above 250 μg mL^{-1} did not decrease the mitochondrial activity of mouse lymphoma cells [68]. Human immortalized T lymphocytes showed no reduction in mitochondrial activity when exposed to 100 μg mL^{-1} of MWCNT-COOH [28]. Therefore, the cellular response to MWCNT-COOHs is specific for each cell type and the exposure conditions.

On the other hand, decreased mitochondrial activity may indicate a change in cell fate. Zhang *et al* [69] have reported that the daughter cell that received older mitochondria during stem cell division tends to differentiate. However, the cell that received new mitochondria maintains its stem cell traits. Thus, it is possible to hypothesize that SHED cells exposed to MWCNT-COOH decrease their metabolic activity due to differentiation process induction. Future studies investigating the osteogenic gene expression and cell mineralization induced by MWCNT-COOH are needed.

Table 1. Carboxylated Multi-wall Carbon Nanotube (MWCNT-COOH) average Hydrodynamic diameter (nm), Polydispersity Index (PDI) and Zeta Potential (mV) obtained by Dynamic Light Scattering

Aqueous Medium	MWCNT-COOH (μg mL^{-1})	Hydrodynamic diameter (nm)	PDI	Zeta Potential (mV)
Deionized Water	0.1	1575.3 ± 957.0	0.9 ± 0.1	0.2 ± 0.9
	1	2989.3 ± 309.1	0.5 ± 0.1	-14.6 ± 2.0
	10	2562.0 ± 477.7	0.9 ± 0.2	-12.6 ± 0.8
	50	5589.0 ± 1. 551.4	0.5 ± 0.4	-21.0 ± 1.0
	100	41250 ± 859.3	0.5 ± 0.3	-18.1 ± 0.8
DMEM/F12	0.1	1198.3 ± 257.8	0.6 ± 0.2	-6.0 ± 0.2
	1	1209.7 ± 204.6	0.7 ± 0.1	-12.2 ± 0.4
	10	2579.3 ± 342.3	0.4 ± 0.1	-9.6 ± 0.7
	50	3752.7 ± 395.7	1.0 ± 0.0	-14.8 ± 0.5
	100	2776.3 ± 310.5	0.2 ± 0.1	-27.8 ± 1.0
DMEM/F12 + FBS	0.1	86.7 ± 36.0	0.3 ± 0.2	-9.3 ± 0.2
	1	90.4 ± 34.5	0.4 ± 0.2	-9.8 ± 1.1
	10	62.7 ± 22.4	0.6 ± 0.2	-11.5 ± 0.9
	50	161.2 ± 54.7	0.8 ± 0.2	-13.1 ± 0.7
	100	211.4 ± 15.7	0.9 ± 0.0	-13.4 ± 0.6

3.4.3 Oxidative stress analysis.

As we observed a mitochondrial activity alteration, and this organelle is responsible for the production of intracellular ROS [70], we next asked if MWCNT-COOH induces stress oxidative on SHED cells. Figure 9 shows no variation ($p>0.05$) in SOD activity in all treatments compared to non-treated cells. The production of ROS is one of the toxicity mechanisms of NMs [2]. These free radicals cause lipid peroxidation of the cell membrane due to the electrostatic interactions between NMs and cells. Hence, NMs can damage cell membranes, entry and interact with organelles and biological macromolecules [71]. However, in the present study, we did not observe changes in the activity of the enzyme SOD, the main antioxidant enzyme in mammals, responsible for neutralizing superoxide anions, fighting oxidative stress, and undesirable effects. These data suggest that the MWCNT-COOH did not alter the redox state of SHEDs grown *in vitro*. Demir & Marcos [68] also reported no change in the percentage of intracellular ROS and no variations in gene expression markers related to oxidative stress in mouse lymphoma cells exposed to concentrations of up to 250 μg mL^{-1} of MWCNT-COOH for 24h. On the other hand, Liu *et al* [72] reported a decrease in SOD enzyme levels in human embryonic lung fibroblasts exposed to MWCNT-COOH concentrations ranging from 5 to 200 μg mL^{-1} for 24h. Song *et al* [18] reported that pristine MWCNT generated more ROS on rat stem cells than functionalized MWCNTs. Therefore, despite the decreased mitochondrial activity, no oxidative stress was observed in SHEDs exposed to MWCNT-COOH.

3.4.4 Cell viability analysis.

We analyzed the cell viability using a flow cytometry assay, marking cells with Propidium Iodide. The results showed that none of the treatments of MWCNT-COOHs altered cell

viability ($p>0.05$) when compared to the non-treated cells (Figure 10, Supplementary Figure 1-3). Similarly, Wu *et al* [25] did not observe cell death in human embryonic kidney cells exposed to 100 μg mL^{-1} MWCNT-COOH for 24 h. On the other hand, MWCNT-COOH (50 and 100 μg mL^{-1}) caused cell death in undifferentiated human monocytes [29].

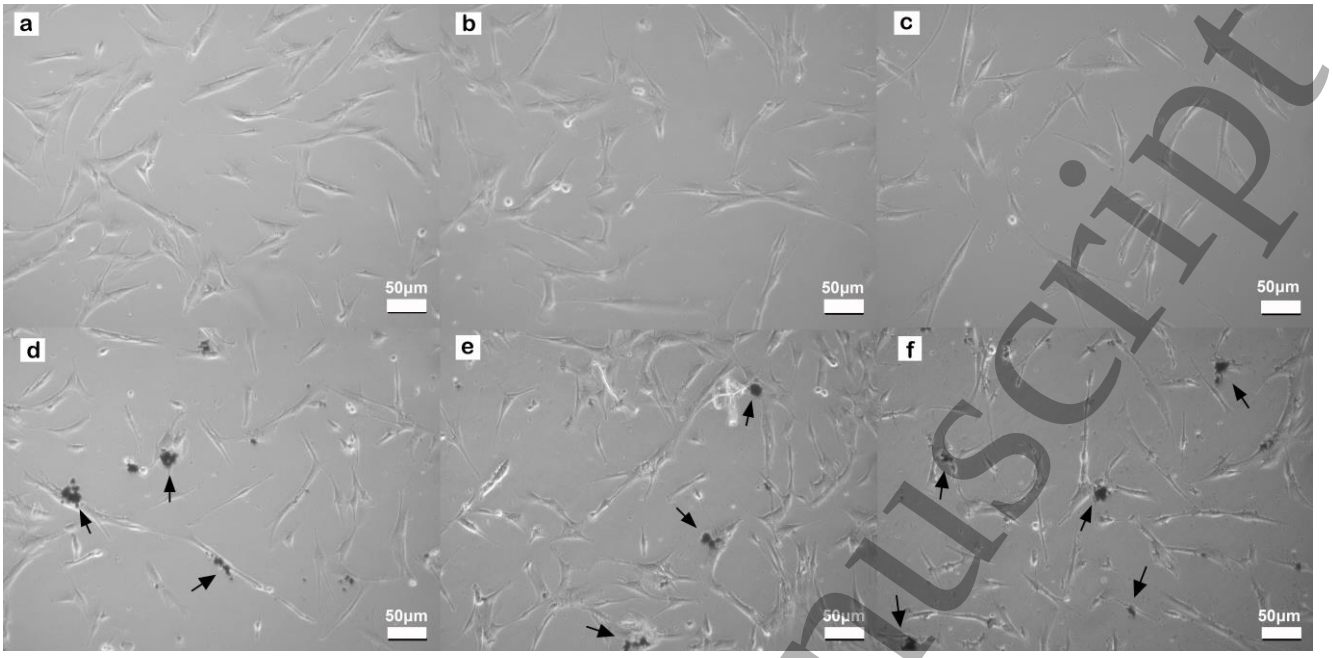

Figure 3. Representative inverted light microscopy images of Stem cells from human exfoliated deciduous teeth (SHED) morphology in adherent monolayer culture at concentrations a) 0 (control), (b) 0.1, (c) 1, (d) 10, (e) 50 and (f) 100 μg mL^{-1} of Carboxylated Multi-wall Carbon Nanotube (MWCNT-COOHs) after 24h of exposure. Arrows signalize MWCNT-COOHs aggregates. Magnification: 10X. Scale bar = 50 μm.

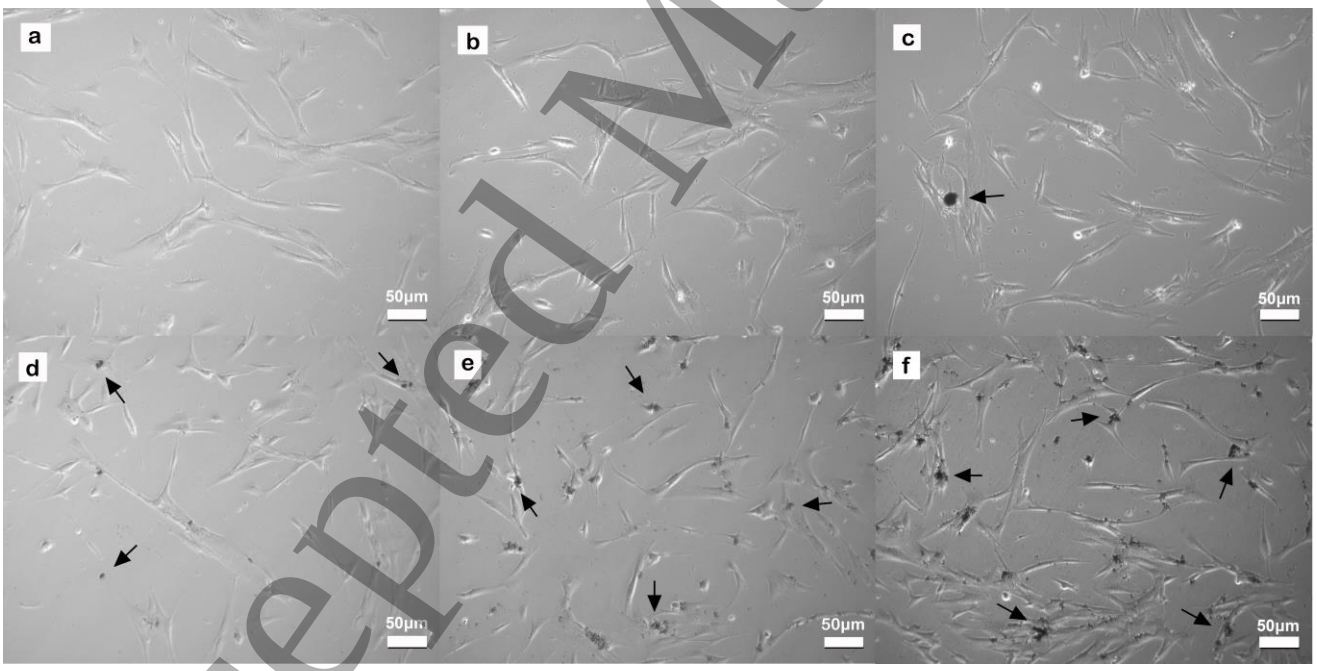

Figure 4. Representative inverted light microscopy images of Stem cells from human exfoliated deciduous teeth (SHED) morphology in adherent monolayer culture at concentrations a) 0 (control), (b) 0.1, (c) 1, (d) 10, (e) 50 and (f) 100 μg mL^{-1} of MWCNT-COOHs after 48h of exposure. Arrows signalize Carboxylated Multi-wall Carbon Nanotube (MWCNT-COOHs) aggregates. Magnification: 10X. Scale bar = 50 μm.

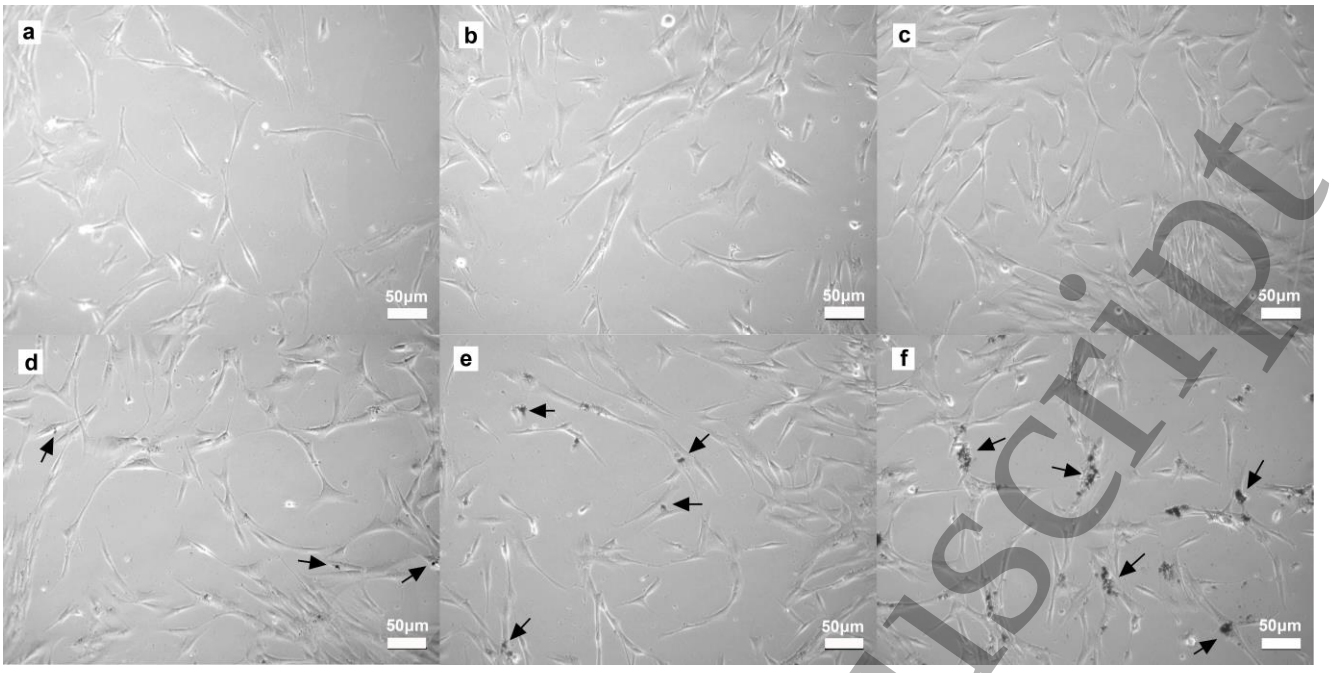

Figure 5. Representative inverted light microscopy images of Stem cells from human exfoliated deciduous teeth (SHED) morphology in adherent monolayer culture at concentrations a) 0 (control), (b) 0.1, (c) 1, (d) 10, (e) 50 and (f) 100 µg mL^{-1} of MWCNT-COOHs after 72h of exposure. Arrows signalize Carboxylated Multi-wall Carbon Nanotube **(**MWCNT-COOHs) aggregates. Magnification: 10X. Scale bar = 50 µm.

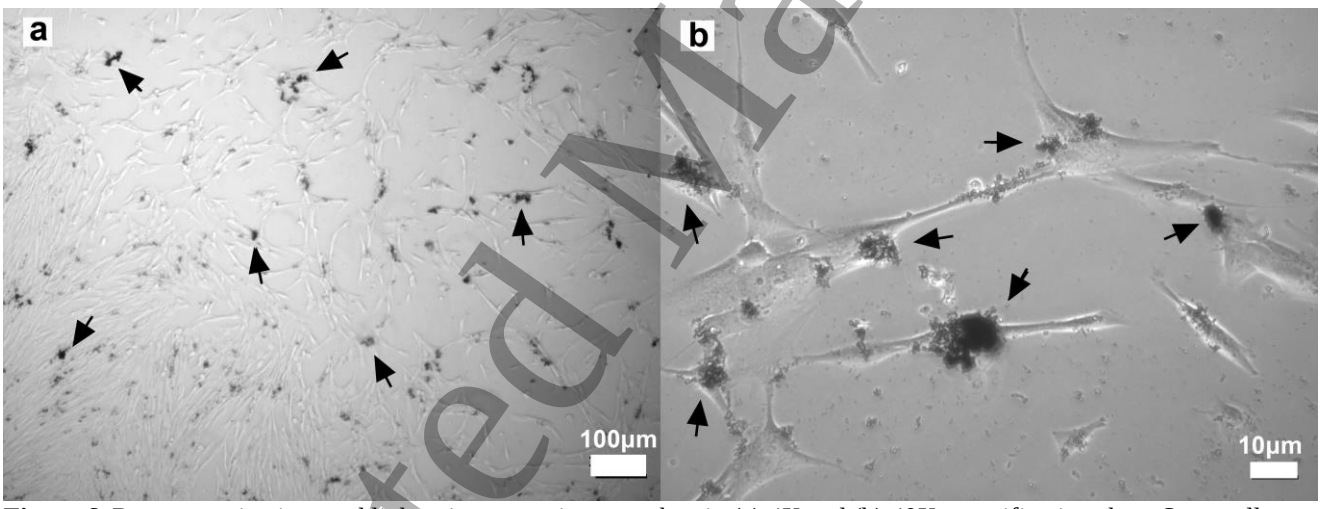

Figure 6. Representative inverted light microscopy images taken in (a) 4X and (b) 40X magnification show Stem cells from human exfoliated deciduous teeth (SHED) growing in adherent monolayer and interacting with aggregates of Carboxylated Multi-wall Carbon Nanotube (MWCNT-COOH) signalized by arrows. Scale bar = 100 e 10 µm.

3.4.5 Genotoxicity Analysis.

The micronucleus frequency is a comprehensive assay for measuring DNA damage and cytostasis involved in genotoxicity. The micronucleus test revealed that SHEDs exposed to MWCNT-COOH for 24h had no change in the frequency of micronuclei when compared to the control group ($p>0.05$) (Table 2). It suggests that this NM does not lead to genomic damage in this cell type. According to the studies by Szendi & Varga [73], human lymphocytes treated with 1 mg mL^{-1} MWCNT showed no increase in the frequency of micronuclei. On the other hand, MWCNT induced micronucleus production in rat lung epithelial cells [74]. A previous study showed that functionalized and non-functionalized MWCNT also increased micronuclei frequency in human dermal fibroblast cells [75]. Thus, considering that micronuclei are a consequence of the formation of DNA fragments or extra chromosomes, the results of this study indicate that MWCNT-COOH did not present genotoxic effects in SHED cells. The divergence of

the present data compared to that reported in the literature may be related to the fact that different cell types vary in their metabolic activities, cell surface receptors, and DNA repair mechanisms [76]. Therefore, the mechanisms of nanogenotoxicity are also variable among cell types. Besides, absorption, distribution, metabolism, and toxicity of carbon nanotubes depend on their physicochemical properties, such as functionalization, size, aggregation, and purity [77]. The oxidation and amination for functionalization of MWCNTs can reduce metals content from NMs synthesis [78]. Therefore, this may be an additional contributing factor to the cytocompatibility observed in the present study.

We show the Cytokines Block Proliferation Index (CBPI) values in table 2. The CBPI is calculated based on the number of mononucleated, binucleated, and multinucleated cells found in the slides. A decrease in this index value indicates a loss in cellular functions and/or cell death [31]. This study verified that CBPI of SHED cells coincubated with MWCNT-COOH for 24h did not differ from the control group ($p>0.05$). Binucleated cells were observed in all treatments, with micronuclei in some of them (Figure 11). Therefore, the analysis of the CBPI values shows that the cells were in the process of cell division, confirming cell viability results by flow cytometry. This result is also in agreement with the result of the SOD assay, considering that cells cannot be under oxidative stress for proliferation [70].

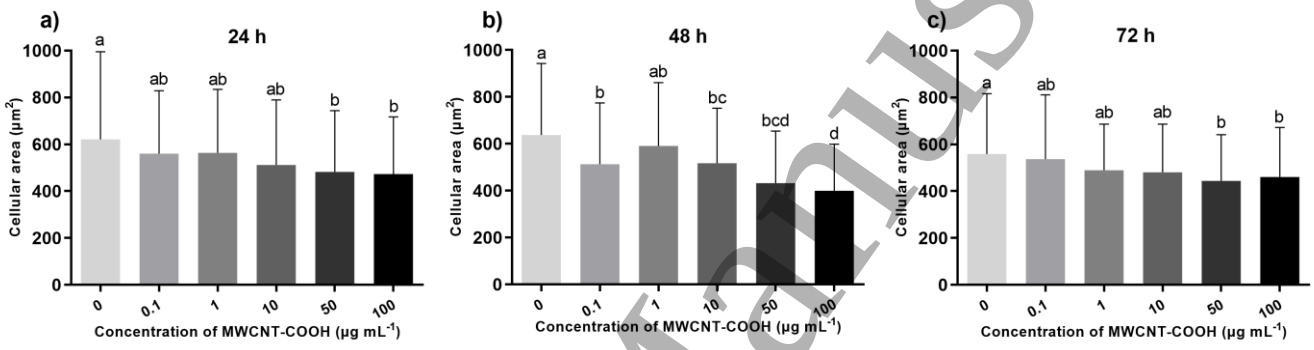

Figure 7. Averages of the cellular area in μm^2 as a function of dose and time of exposure to Carboxylated Multi-wall Carbon Nanotube (MWCNT-COOH). The cellular area was manually measured using the ImageJ (Wayne Rasband) software, n= 100. Averages that do not differ from each other ($p>0.05$) in Tukey's test are represented by the same letters.

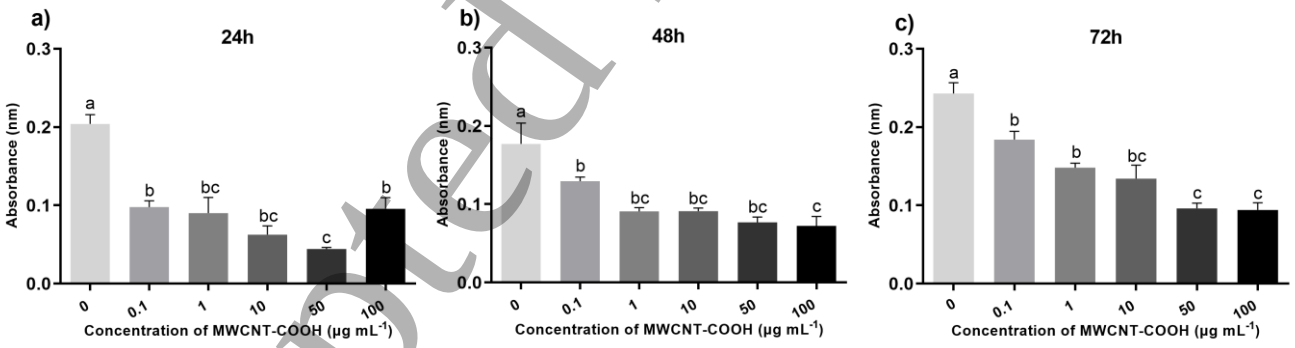

Figure 8. Mitochondrial activity analysis via thiazolyl blue tetrazolium blue (MTT) assay (a) 24 hours, (b) 48h, (c) 72h after Stem cells from human exfoliated deciduous teeth (SHED) treatment with Carboxylated Multi-wall Carbon Nanotube (MWCNT-COOH). The experiments were performed in six replicates and repeated two times. The same letters represent averages that do not differ ($p > 0.05$) in Tukey's test.

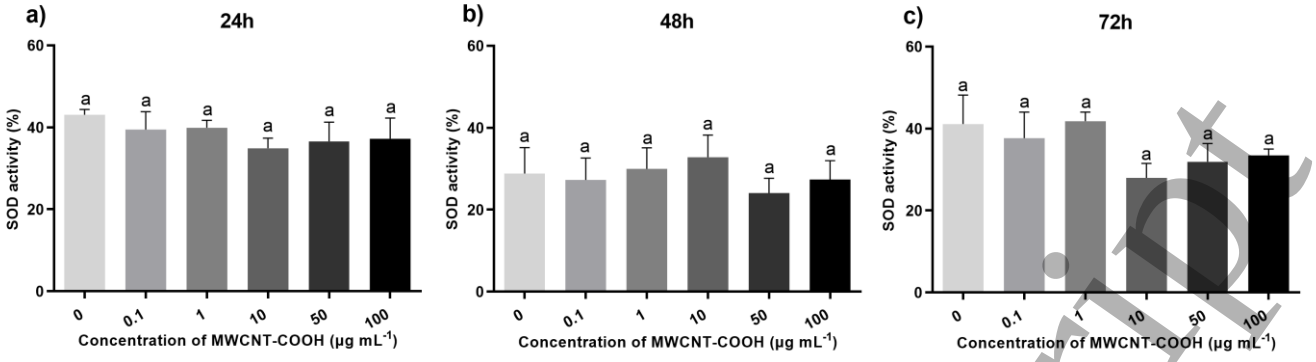

Figure 9. Oxidative stress analysis was assessed through superoxide dismutase (SOD) activity assay for (a) 24h, (b) 48h, (c) 72h after SHEDs treatment with Carboxylated Multi-wall Carbon Nanotube (MWCNT-COOH). The experiments were performed in triplicates and repeated two times. The same letters represent averages that do not differ ($p > 0.05$) in Tukey's test.

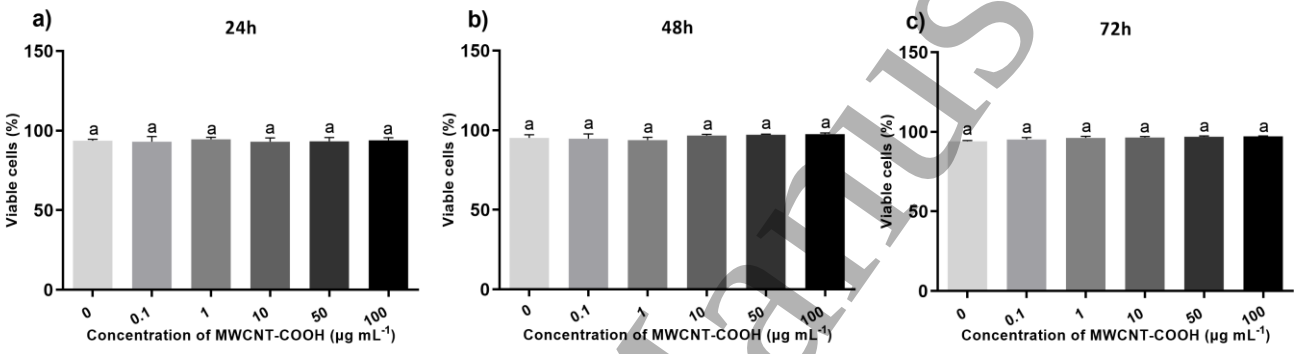

Figure 10. Statistical analysis of cell viability evaluated by flow cytometry with propidium iodide marking for (a) 24h, (b) 48h, (c) 72h of Stem cells from human exfoliated deciduous teeth (SHED) coincubation with 0 (control), 0.1, 1, 10, 50 and 100 µg mL^{-1} of Carboxylated Multi-wall Carbon Nanotube (MWCNT-COOH). The experiments were performed in duplicates and repeated two times. Averages that do not differ from each other ($p > 0.05$) in Tukey's Test are represented by the same lette

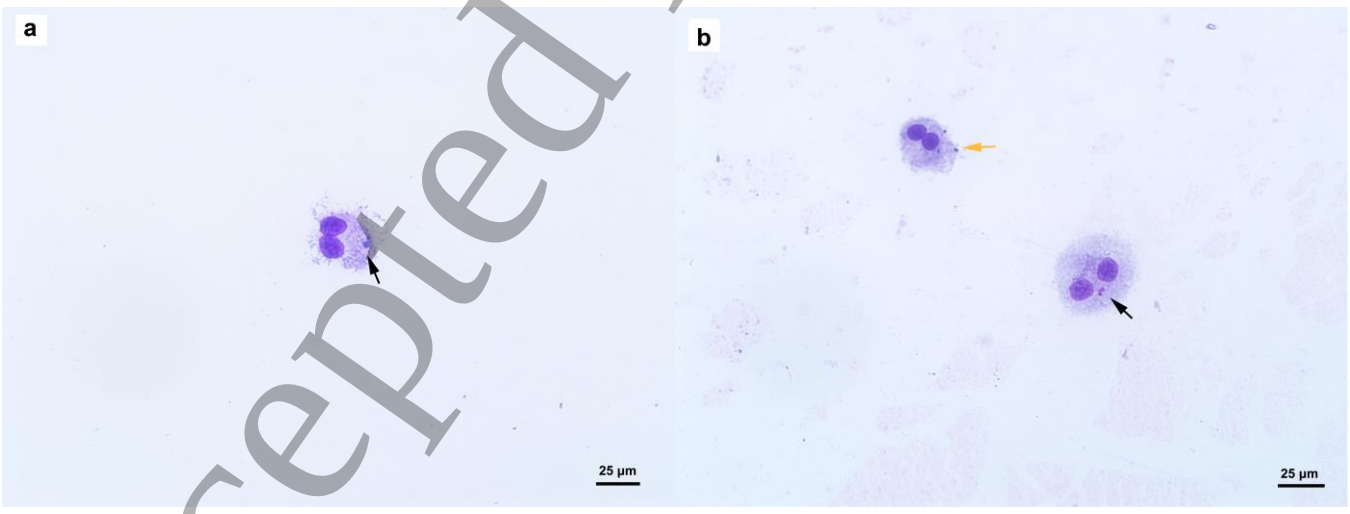

Figure 11. Representation of micronuclei assay in Stem cells from human exfoliated deciduous teeth (SHED) exposed to (a) 0 (control) and (b) 50 µg mL-1 of Carboxylated Multi-wall Carbon Nanotube (MWCNT-COOH) for 24 h. Black arrows indicate micronucleus in binucleated cells, and orange arrow indicate MWCNT-COOH aggregate. Magnification: 20 X. Scale bar = 25 µm.

Table 2. Micronucleus frequency and Cytokinesis-block proliferation index (CBPI) for genotoxicity evaluation of Stem cells from human exfoliated deciduous teeth (SHED) treated with Carboxylated Multi-wall Carbon Nanotube (MWCNT-COOHs) for 24h. Data are shown as the mean and standard error of the average frequency of micronuclei. According to the chi-square test, micronuclei frequency did not differ from the control ($p > 0.05$). The experiments were performed in triplicates and repeated two times, n = 2000.

Treatments MWCNT-COOH (μg mL^{-1})	Micronuclei (%)	CBPI value (%)
0 (control)	2.7 ± 1.4	1.59
0.1	7.3 ± 1.8	1.58
1	4.7 ± 0.3	1.60
10	5.3 ± 2.8	1.63
50	6.3 ± 1.8	1.58
100	2.6 ± 0.8	1.60

4. Conclusions

In conclusion, our findings reveal that MWCNT-COOH has good cytocompatibility with SHED cells. According to the experimental conditions, MWCNT-COOH did not change the area of the cell spreading at low concentrations (0.1, 1 and 10 μg mL^{-1}) after 24 and 72h time exposure, except at higher concentrations (50 and 100 μg mL^{-1}). Despite reducing mitochondrial activity, the SOD assay showed that MWCNT-COOHs did not cause oxidative stress in the SHEDs. The MWCNT-COOH did not decrease the cell viability and did not cause genotoxicity. Our work evaluated some toxicological parameters of MWCNT-COOH in SHED cells, providing essential information for future safe applications of this NM in regenerative dentistry and medicine.

Acknowledgments

We would like to thank Dr. Elyabe Monteiro de Matos his help with Flow Cytometry analysis and MSc. Camila Kauany da Silva Azevedo for her help with Fourier Transformed Infrared analysis. This work was supported by the Fundação de Amparo à Pesquisa do Estado de Minas Gerais (FAPEMIG) [grant number APQ-02342-17], the Rede Mineira de Pesquisa e Inovação para Bioengenharia de Nanossistemas (RM PI-BEM) [grant number TEC - RED-00282-16], Conselho Nacional de Desenvolvimento Científico e Tecnológico (CNPq) [grant number 433461/2018-7], Rede de Nanotecnologia Aplicada ao Agronegócio (AGRONANO), Coordenação de Aperfeiçoamento de Pessoal de Nível Superior (CAPES) and Pós-Graduação em Ciências Biológicas (PPGCBIO-UFJF).

REFERENCES

[1] Wang W, Yue X, Huang H, Wang C, Mo D, Wu Y, Xu Q, Zhou C, Zhu H and Zhang C 2019 Electrical resistance prediction for functionalized multi-walled carbon nanotubes/epoxy resin composite gasket under thermal creep conditions *Materials (Basel).* **12** 2704.

[2] Yu Z, Li Q, Wang J, Yu Y, Wang Y, Zhou Q and Li P 2020 Reactive oxygen species-related nanoparticle toxicity in the biomedical field *Nanoscale Res. Lett.* **15** 115

[3] Jha M K, Hata K and Subramaniam C 2019 Interwoven carbon nanotube wires for high-performing, mechanically robust, washable, and wearable supercapacitors *ACS Appl Mater Interfaces* **11** 18285–94

[4] Menezes B R C de, Rodrigues K F, Fonseca B C D S, Ribas R G, Montanheiro T L D A and Thim G P 2019 Recent advances in the use of carbon nanotubes as smart biomaterials *J. Mater. Chem. B* **7** 1343–60

[5] Rahman G, Najaf Z, Mehmood A, Bilal S, Shah A, Mian S and Ali G 2019 An overview of the recent progress in the synthesis and applications of carbon nanotubes *Carbon Res.* **5** 3

[6] Raphey V R, Henna T K, Nivitha K P, Mufeedha P, Sabu C and Pramod K 2019 Advanced biomedical applications of carbon nanotube *Mater. Sci. Eng. C Mater. Biol. Appl.* **100** 616–30

[7] Basu A K, Sah A N, Pradhan A and Bhattacharya S 2019 Poly-L-Lysine functionalised MWCNT-rGO nanosheets based 3-d hybrid structure for femtomolar

level cholesterol detection using cantilever based sensing platform *Sci. Rep.* **9** 3686

[8] Munk M, Ladeira L O, Carvalho B C, Camargo L S A, Raposo N R B, Serapião R V, Quintão C C R, Silva S R, Soares J S, Jorio A and Brandão H M 2016 Efficient delivery of DNA into bovine preimplantation embryos by multiwall carbon nanotubes *Sci. Rep.* **6** 33588

[9] Munk M, de Souza Salomão Zanette R, de Almeida Camargo L S, de Souza N L G D, de Almeida C G, Gern J C, de Sa Guimaraes A, Ladeira L O, de Oliveira L F C and de Mello Brandão H 2017 Using carbon nanotubes to deliver genes to hard-to-transfect mammalian primary fibroblast cells *Biomed. Phys. Eng. Express.* **3** 045002

[10] Seyfoori A, Sarfarazijami S and Seyyed Ebrahimi S A 2019 pH-responsive carbon nanotube-based hybrid nanogels as the smart anticancer drug carrier *Artif. Cells Nanomed. Biotechnol.* **47** 1437–43

[11] Hassan H A F M, Smyth L, Wang J T W, Costa P M, Ratnasothy K, Diebold S S, Lombardi G and Al-Jamal K T 2016 Dual stimulation of antigen presenting cells using carbon nanotube-based vaccine delivery system for cancer immunotherapy *Biomaterials* **104** 310–22

[12] Huang B, Vyas C, Roberts I, Poutrel Q A, Chiang W H, Blaker J J, Huang Z and Bártolo P 2019 Fabrication and characterisation of 3D printed MWCNT composite porous scaffolds for bone regeneration *Mater. Sci. Eng. C Mater. Biol. Appl.* **98** 266–78

[13] Hasanzadeh E, Ebrahimi-Barough S, Mirzaei E, Azami M, Tavangar S M, Mahmoodi N, Basiri A and Ai J 2019 Preparation of fibrin gel scaffolds containing MWCNT/PU nanofibers for neural tissue engineering *J. Biomed. Mater. Res. A* **107** 802–814

[14] Sukhanova A, Bozrova S, Sokolov P, Berestovoy M, Karaulov A and Nabiev I 2018 Dependence of nanoparticle toxicity on their physical and chemical properties *Nanoscale Res. Lett.* **13** 44

[15] Prajapati S K, Malaiya A, Kesharwani P, Soni D and Jain A 2020 Biomedical applications and toxicities of carbon nanotubes *Drug Chem. Toxicol.* **7** 1–16

[16] Falinski M M, Garland M A, Hashmi S M, Tanguay R L and Zimmerman J B 2019 Establishing structure-property-hazard relationships for multi-walled carbon nanotubes: The role of aggregation, surface charge, and oxidative stress on embryonic zebrafish mortality *Carbon* **155** 587–600

[17] Palmer B C, Phelan-Dickenson S J and Delouise L A 2019 Multi-walled carbon nanotube oxidation dependent keratinocyte cytotoxicity and skin inflammation *Part. Fibre Toxicol.* **16** 3

[18] Song G, Guo X, Zong X, DU L, Zhao J, Lai C and Jin X 2019 Toxicity of functionalized multi-walled carbon nanotubes on bone mesenchymal stem cell in rats. *Dent. Mater. J.* **8** 127–135

[19] Mia MB and Saxena RK 2021 Toxicity of poly-dispersed single-walled carbon nanotubes on bone marrow derived hematopoietic stem and progenitor cells. *Curr. Res. Toxicol.* **2** 82–92

[20] Mooney E, Dockery P, Greiser U, Murphy M and Barron V 2008 Carbon nanotubes and mesenchymal stem cells: biocompatibility, proliferation and differentiation. *Nano Lett.* **8** 2137–43

[21] Das K, Madhusoodan AP, Mili B, Kumar A, Saxena AC, Kumar K, Sarkar M, Singh P, Srivastava S and Bag S 2017 Functionalized carbon nanotubes as suitable scaffold materials for proliferation and differentiation of canine mesenchymal stem cells *Int. J. Nanomedicine.* **12** 3235–3252

[22] Kroustalli A and Deligianni D 2016 Carbon nanotube surface regular topography improves cell response, depending on cell passage *Bone Tissue Regener. Insights*. **7**

[23] Lee J-R, Ryu S, Kim S and Kim B S 2015 Behaviors of stem cells on carbon nanotube *Biomaterials Research* **19** 3

[24] Yao X, Yin N and Faiola F 2016 Stem cell toxicology: a powerful tool to assess pollution effects on human health *Natl. Sci. Rev.* **3** 4

[25] Wu L, Zhang Y, Zhang C, Cui X, Zhai S, Liu Y, Li C, Zhu H, Qu G, Jiang G and Yan B 2014 Tuning cell autophagy by diversifying carbon nanotube surface chemistry *ACS Nano* **8** 2087–99

[26] Ursini C L, Maiello R, Ciervo A, Fresegna A M, Buresti G, Superti F, Marchetti M, Iavicoli S and Cavallo D 2016 Evaluation of uptake, cytotoxicity and inflammatory effects in respiratory cells exposed to pristine and -OH and -COOH functionalized multi-wall carbon nanotubes *J. Appl. Toxicol.* **36** 394–403

[27] Aminzadeh Z, Jamalan M, Chupani L, Lenjannezhadian H, Ghaffari M A, Aberomand M and Zeinali M 2017 In vitro reprotoxicity of carboxyl-functionalised single- and multi-walled carbon nanotubes on human spermatozoa *Andrologia* **49**

[28] Lotfipanah S, Zeinali M and Yaghmaei P 2019 Induction of caspase-2 gene expression in carboxyl-functionalized carbon nanotube-treated human T-cell leukemia (Jurkat) cell line *Drug Chem. Toxicol.* **44** 394–9

[29] Gallud A, Delaval M, Kinaret P, Marwah VS, Fortino V, Ytterberg J, Zubarev R, Skoog T, Kere J, Correia M, Loeschner K, Al-Ahmady Z, Kostarelos K, Ruiz J, Astruc D, Monopoli M, Handy R, Moya S, Savolainen K, Alenius H, Greco D and Fadeel B 2020 Multiparametric profiling of engineered nanomaterials: unmasking the surface coating effect. *Adv. Sci.* **7** 2002221

[30] Braun EI, Draper R, Pantano P 2016 Enriched surface acidity for surfactant-free suspensions of carboxylated carbon nanotubes purified by centrifugation *Analytical Chem. Res*. **8** 26-33.

[31] Ferreira LS, Diniz IMA, Maranduba CMS, Miyagi SPH, Rodrigues MFSD, Moura-Netto C, Marques MM 2019 Short-term evaluation of photobiomodulation therapy on the proliferation and undifferentiated status of dental pulp stem cells *Lasers Med. Sci.* **34** 659–66

[32] Standardization, ISO. 10993-5. Biological compatibility of medical devices, in Part 5. Tests for cytotoxicity In Vitro Methods. 2009: Geneve.

[33] OECD. Test No. 487: In Vitro Mammalian Cell Micronucleus Test. OECD, 2016

[34] van Trinh P, Anh N N, Tam N T, Hong N T, Hong P N, Minh P N and Thang B H 2017 Influence of defects induced by chemical treatment on the electrical and thermal conductivity of nanofluids containing carboxyl-functionalized multi-walled carbon nanotubes *RSC Advances* **7** 49937–46

[35] Yao MZ, Hu YL, Sheng XX, Lin J, Ling D, Gao JQ 2016 Toxicity analysis of various Pluronic F-68-coated carbon nanotubes on mesenchymal stem cells. *Chem-biolog. Interact.* 250 47-58.

[36] Bai W, Wu Z, Mitra S and Brown J M 2016 Effects of multiwalled carbon nanotube surface modification and purification on bovine serum albumin binding and biological responses *J. Nanomater.* **2016** 2159537

[37] Zhao Z, Yang Z, Hu Y, Li J and Fan X 2013 Multiple functionalization of multi-walled carbon nanotubes with carboxyl and amino groups *Appl. Surf. Sci.* **276** 476–81

[38] Montanheiro T L D A, Cristóvan F H, Machado J P B, Tada D B, Durán N and Lemes A P 2014 Effect of MWCNT functionalization on thermal and electrical properties of PHBV/MWCNT nanocomposites *J. Mater. Res.* **30** 55–65

[39] Tan J M, Karthivashan G, Arulselvan P, Fakurazi S and Hussein M Z 2014 Characterization and in vitro sustained release of silibinin from pH responsive carbon nanotube-based drug delivery system *J. Nanomater.* **2014** 439873

[40] Mishra S K, Tripathi S N, Choudhary V and Gupta B D 2015 Surface plasmon resonance-based fiber optic methane gas sensor utilizing graphene-carbon nanotubes-poly(methyl methacrylate) hybrid nanocomposite *Plasmonics* **10** 1147–57

[41] Mallakpour S, Dinari M and Behranvand V 2014 Anionic clay intercalated by multi-walled carbon nanotubes as an efficient 3D nanofiller for the preparation of high-performance l-alanine amino acid containing poly(amide-imide) nanocomposites *J. Mater. Sci.* **49** 7004–13

[42] Jorio A, Pimenta MA, Souza Filho AG, Samsonidze GG, Swan AK, Unlü MS, Goldberg BB, Saito R, Dresselhaus G and Dresselhaus MS 2003 Resonance Raman spectra of carbon nanotubes by cross-polarized light *Phys. Rev. Lett.* **90** 107403

[43] Murphy H, Papakonstantinou P and Okpalugo T I T 2006 Raman study of multiwalled carbon nanotubes functionalized with oxygen groups *J. Vac. Sci. Technol. B: Microelectron. Nanometer Struc. Process* **24** 715

[44] Wepasnick K A, Smith B A, Schrote K E, Wilson H K, Diegelmann S R and Fairbrother D H 2011 Surface and structural characterization of multi-walled carbon nanotubes following different oxidative treatments *Carbon* **49** 24–36

[45] Silva W M, Ribeiro H, Seara L M, Calado H D R, Ferlauto A S, Paniago R M, Leite C F and Silva G G 2012 Surface properties of oxidized and aminated multi-walled carbon nanotubes *J. Braz. Chem. Soc.* **23** 1078–86

[46] Rebelo S L H, Guedes A, Szefczyk M E, Pereira A M, Araújo J P and Freire C 2016 Progress in the Raman spectra analysis of covalently functionalized multiwalled carbon nanotubes: Unraveling disorder in graphitic materials *Phys. Chem. Chem. Phys.* **18** 12784–96

[47] Munk M, Zanette R S S, Camargo L S A, Souza N L G D, Almeida C G, Gern J C, Guimaraes A S, Ladeira L O, Oliveira L F C and Brandão H M 2017 Using carbon nanotubes to deliver genes to hard-to-transfect mammalian primary fibroblast cells *Biomed. Phys. Eng. Express.* **3** 045002

[48] Omrani A N, Esmaeilzadeh E, Jafari M and Behzadmehr A 2019 Effects of multi walled carbon nanotubes shape and size on thermal conductivity and viscosity of nanofluids *Diam. Relat. Mater.* **93** 96–104

[49] Kumar P, Choonara Y E, du Toit L C, Modi G, Naidoo D and Pillay V 2012 Novel high-viscosity polyacrylamidated chitosan for neural tissue engineering: Fabrication of anisotropic neurodurable scaffold via molecular disposition of persulfate-mediated polymer slicing and complexation International *Int. J. Mol. Sci.* **13** 13966–84

[50] Li C, Wang L, Yang Z, Kim G, Chen H and Ge Z 2012 A viscoelastic chitosan-modified three-dimensional porous poly(L-lactide-co-ε-caprolactone) scaffold for cartilage tissue engineering *J. Biomater. Sci. Polym. Ed.* **23** 405–24

[51] Rodríguez-Vázquez M, Vega-Ruiz B, Ramos-Zúñiga R, Saldaña-Koppel D A and Quiñones-Olvera L F 2015 Chitosan and its potential use as a scaffold for tissue engineering in regenerative medicine *BioMed Res. Int.* **2015** 821279

[52] Lee J, Kim M, Hong C K and Shim S E 2007 Measurement of the dispersion stability of pristine and surface-modified multiwalled carbon nanotubes in various nonpolar and polar solvents *Meas. Sci. Technol.* **18** 3707–12

[53] Lima T, Bernfur K, Vilanova M and Cedervall T 2020 Understanding the lipid and protein corona formation on different sized polymeric nanoparticles *Sci. Rep.* **10** 1129

[54] Zhang T, Tang M, Yao Y, Ma Y and Pu Y 2019 MWCNT interactions with protein: Surface-induced changes in protein adsorption and the impact of protein corona on cellular uptake and cytotoxicity *Int. J. Nanomedicine* **14** 993–1009

[55] Baek Y W and An Y J 2011 Microbial toxicity of metal oxide nanoparticles (CuO, NiO, ZnO, and Sb2O3) to Escherichia coli, Bacillus subtilis, and Streptococcus aureus *Sci. Total Environ.* **409** 1603–8

[56] Levard C, Mitra S, Yang T, Jew A D, Badireddy A R, Lowry G v. and Brown G E 2013 Effect of chloride on the dissolution rate of silver nanoparticles and toxicity to E. coli *Environ. Sci. Technol.* **47** 5738–45

[57] Baalousha M, Sikder M, Prasad A, Lead J, Merrifield R and Chandler G T 2016 The concentration-dependent behaviour of nanoparticles *Environ. Chem.* **13** 1–3

[58] Danaei M, Dehghankhold M, Ataei S, Hasanzadeh Davarani F, Javanmard R, Dokhani A, Khorasani S and Mozafari M R 2018 Impact of particle size and polydispersity index on the clinical applications of lipidic nanocarrier systems *Pharmaceutics* **10** 1–17

[59] Hamilton R F, Wu Z, Mitra S and Holian A 2018 The effects of varying degree of MWCNT carboxylation on bioactivity in various in vivo and in vitro exposure models *Int. J. Mol. Sci.* **19** 354

[60] Hamilton R F, Wu Z, Mitra S, Shaw P K and Holian A 2013 Effect of MWCNT size, carboxylation, and purification on in vitro and in vivo toxicity, inflammation and lung pathology *Part. Fibre Toxicol.* **10** 57

[61] Zeinabad H A, Zarrabian A, Saboury A A, Alizadeh A M O and Falahati M 2016 Interaction of single and multi wall carbon nanotubes with the biological systems: Tau protein and PC12 cells as targets *Sci. Rep.* **6** 26508

[62] Amaral D L A S, Zanette R S S, Almeida C G, Almeida L B F, Oliveira L F C D, Marcomini R F, Nogueira B V, Santos M O, Brandao H M, Maranduba C M C and Munk M 2019 In vitro evaluation of barium titanate nanoparticle/alginate 3D scaffold for osteogenic human stem cell differentiation *Biomed. Mater.* **14** 035011

[63] Pérez-Luna V, Moreno-Aguilar C, Arauz-Lara J L, Aranda-Espinoza S and Quintana M 2018 Interactions of functionalized multi-wall carbon nanotubes with giant phospholipid vesicles as model cellular membrane system *Sci. Rep.* **8** 17998

[64] Kino-oka M, Maeda Y, Sato Y, Maruyama N, Takezawa Y, Khoshfetrat A B, Sugawara K and Taya M 2009 Morphological evaluation of chondrogenic potency in passaged cell populations *J. Biosci. Bioeng.* **107** 544–51

[65] Kelly D J and Jacobs C R 2010 The role of mechanical signals in regulating chondrogenesis and osteogenesis of mesenchymal stem cells *Birth Defects Res. C Embryo Today* **90** 75–85

[66] Matsuoka F, Takeuchi I, Agata H, Kagami H, Shiono H, Kiyota Y, Honda H and Kato R 2013 Morphology-based prediction of osteogenic differentiation potential of human mesenchymal stem cells *PLoS ONE* **8** e55082

[67] Chen Y-S and Hsiue G-H 2013 Directing neural differentiation of mesenchymal stem cells by carboxylated multiwalled carbon nanotubes *Biomaterials* **34** 4936–44

[68] Demir E and Marcos R 2018 Toxic and genotoxic effects of graphene and multi-walled carbon nanotubes *J. Toxicol. Environ. Health A* **81** 645–60

[69] Zhang H, Menzies K J and Auwerx J The role of mitochondria in stem cell fate and aging *Development* **145** 143420

[70] Antico Arciuch V G, Elguero M E, Poderoso J J and Carreras M C 2012 Mitochondrial regulation of cell cycle and proliferation *Antioxid. Redox Signal.* **16** 1150–80

[71] Hou J, Wang L, Wang C, Zhang S, Liu H, Li S and Wang X 2019 Toxicity and mechanisms of action of titanium dioxide nanoparticles in living organisms *J. Environ. Sci.* **75** 40–53

[72] Liu S, Chen J, Zhang K, Wu S, Liu R and Gao X 2014 Cytotoxicity of carboxyl carbon nanotubes on human embryonic lung fibroblast cells and its mechanism *J. Exp. Nanosci.* **9** 210–20

[73] Szendi K and Varga C 2008 Lack of genotoxicity of carbon nanotubes in a pilot study *Anticancer Res.* **28** 349–52

[74] Muller J, Decordier I, Hoet P H, Lombaert N, Thomassen L, Huaux F, Lison D and Kirsch-Volders M 2008 Clastogenic and aneugenic effects of multi-wall carbon nanotubes in epithelial cells *Carcinogenesis* **29** 427–33

[75] Patlolla A, Patlolla B and Tchounwou P 2010 Evaluation of cell viability, DNA damage, and cell death in normal human dermal fibroblast cells induced by functionalized multiwalled carbon nanotube *Mol. Cell. Biochem.* **338** 225–32

[76] Vevers W F and Jha A N 2008 Genotoxic and cytotoxic potential of titanium dioxide (TiO2) nanoparticles on fish cells in vitro *Ecotoxicology* **17** 410–20

[77] Lindberg H K, Falck G C M, Suhonen S, Vippola M, Vanhala E, Catalán J, Savolainen K and Norppa H 2009 Genotoxicity of nanomaterials: DNA damage and micronuclei induced by carbon nanotubes and graphite nanofibres in human bronchial epithelial cells in vitro *Toxicol. Lett.* **186** 166–73

[78] Vuković G, Marinković A, Obradović M, Radmilović V, Čolić M, Aleksić R and Uskoković P S 2009 Synthesis, characterization and cytotoxicity of surface amino-functionalized water-dispersible multi-walled carbon nanotubes *Appl. Surf. Sci.* **255** 8067–75